Nitranions and Their Precursors: Charge Density Rearrangements and ^{15}N NMR Chemical Shift Changes

Carlo Gatti,*,† Alessandro Ponti,‡ Aldo Gamba,‡ and Giorgio Pagani§

Contribution from Centro CNR per lo Studio delle Relazioni tra Struttura e Reattivita' Chimica, via C. Golgi 19, 20133 Milano, Italy, and Dipartimento di Chimica Fisica ed Elettrochimica and Dipartimento di Chimica Organica e Industriale, Universita' degli Studi di Milano, via C. Golgi 19, 20133 Milano, Italy. *Received December 3, 1990*

Abstract: RPA LORG (random phase approximation, localized orbitals-local origin) calculations of the changes in the ^{15}N nuclear magnetic shielding tensor occurring upon deprotonation of pyridinium cation, and of a number of nitranion precursors, shed light on the corresponding changes in the experimental isotropic ^{15}N chemical shifts. The downfield shift of deprotonated nitrogens results from the dominance of the decrease in shielding in the molecular plane over the concurrent increase (or near constancy) of the out-of-plane shielding. Conversely, the upfield shift of pyridyl nitrogens, with respect to nitranion precursors, is due to the dominance of the increase in the molecular-plane shielding over the decrease in the out-of-plane shielding. The charge density rearrangements occurring upon deprotonation are rationalized in terms of the relevant RHF/6-31G+ charge density topologies, within the framework of the *quantum theory of atoms in molecules*. Deprotonation of a planar tricoordinated nitrogen increases its σ population and allows an efficient release of its π charge to the ring π system. The σ density made available upon deprotonation at nitrogen is to a great extent transferred to the whole molecular σ framework. The removal of π charge allows the amino nitrogen to effectively conjugate to the ring π system or, in the case of pyrrole anion and pyridine, to realize π conjugation throughout the heterocyclic ring. These mechanisms are evidenced by changes in the Laplacian of the charge density, and in the preferred direction of charge accumulation along the N–C bond, following deprotonation. The correlation between the charge density redistribution mechanisms and the changes in shielding tensor components are highlighted. Empirical relationships between the electron populations and the ^{15}N NMR shifts are investigated for both virial partitioning (VP) and Mulliken partitioning (MP) charges. ^{15}N NMR shifts correlate with both σ and π VP charges, but not with their sum. Correlations between anisotropies in shielding and anisotropies in charge distribution are discussed. The reasons for the existence of correlations also involving isotropic shielding are given.

I. Introduction

Over the last decade increasing attention has been devoted to ^{15}N NMR,[1] owing to its importance in chemical[2] and biological[3] investigations. In particular, ^{15}N NMR spectroscopy has proved to be an ideal tool for the study of nitranions, whose role as key intermediates in organic synthesis is widely acknowledged.[4] However, the effect of geometrical relaxation and charge rearrangement on the chemical shift variation upon deprotonation of nitranion precursors has not been thoroughly explored and is worthy of further investigation. Empirical relationships between atomic charges and NMR shifts have been found to be particularly useful in providing atomic charge values and charge-related molecular properties. Unfortunately, these correlations lack any clear theoretical basis.[5] Also, their validity is often limited to a given series of molecules, and they should not be used indiscriminately; up- or downfield shifts with increasing electron population are encountered,[6-8] depending on the type of system under study. Indeed, Comeau[8] and Escudero[9] have proposed linear relationships between ^{15}N NMR shifts and atomic populations resembling those found for ^{13}C and ^{17}O,[6,7] for corresponding classes of systems. However, no charge–shift relationship has been proposed for nitranions so far.

Previous experimental studies[11,12] of nitranions of pyrrole and aromatic and heteroaromatic amines demonstrate that the deprotonation-induced ^{15}N displacement is to low field for deprotonated nitrogen and to high field for pyridyl nitrogen. Molecules were studied in which the nitrogen atom is part of a π-conjugated system, to avoid rehybridization, and the following conclusions[12] were deduced. (a) Deprotonation of a planar tricoordinated nitrogen acid places the electron pair in an sp^2 orbital, increases the nitrogen σ electron population (P_σ^N), and accordingly induces a downfield shift for this nitrogen. (b) If the P_σ^N increase can be partly counterbalanced by a π charge release into the p orbital of the trigonal dicoordinated nitrogen atom, the latter undergoes an upfield shift due to an increase in its π population (P_π^N). (c) The dichotomy in observed shift behavior can be rationalized in terms of the symmetry of the orbital in which the electron pair is generated or that to which it is localized.

However, these conclusions were drawn on the basis of experimental data only. Therefore, neither an evaluation of P_σ versus P_π changes nor any study of the mechanism of σ and π charge redistribution on deprotonation was possible. This could have led to overly simplistic interpretations. Indeed, essential to the orbital theory of electronic structure is the property of self-consistency—that each orbital be determined by its average re-

† Centro CNR.
‡ Dipartimento di Chimica Fisica ed Elettrochimica.
§ Dipartimento di Chimica Organica e Industriale.

(1) Levy, G. C.; Lichter, R. *Nitrogen-15 Nuclear Magnetic Resonance Spectroscopy*; Wiley: New York, 1979. Witanowsky, M.; Stefaniak, L.; Webb, G. A. *Annu. Rep. NMR Spectrosc.* **1986**, *18*, 1.
(2) Philipsborn, W.; Muller, R. *Angew. Chem., Int. Ed. Engl.* **1986**, *25*, 383.
(3) Blomberg, F.; Ruterjans, H. In *Biological Magnetic Resonance*; Berliner, L. J., Reuben, J., Eds.; Plenum Press: New York, 1983; Vol. 5.
(4) Stowell, J. C. *Carbanions in Organic Synthesis*; Wiley: New York, 1979.
(5) (a) Pople, J. A. *J. Chem. Phys.* **1962**, *37*, 53. (b) Vauthier, E. C.; Fliszár, S.; Tonnard, F.; Odiot, S. *Can. J. Chem.* **1983**, *61*, 1417.
(6) Fliszár, S. *Charge Distributions and Chemical Effects*; Springer Verlag: New York, 1983.
(7) (a) Fliszár, S.; Cardinal, G.; Bëraldin, M. T. *J. Am. Chem. Soc.* **1982**, *104*, 5287 and references therein. (b) Farnum, D. G. *Adv. Phys. Org. Chem.* **1975**, *11*, 123. (c) Nelson, G. L.; Williams, E. A. *Prog. Phys. Org. Chem.* **1976**, *12*, 229. (d) Martin, G. J.; Martin, M. L.; Odiot, S. *Org. Magn. Reson.* **1975**, *7*, 2. (e) Hehre, W. J.; Taft, R. W.; Topsom, R. D. *Prog. Phys. Org. Chem.* **1976**, *12*, 159. (f) Olah, G. A.; Westerman, P. W. *J. Am. Chem. Soc.* **1973**, *95*, 7530.
(8) Comeau, M.; Bëraldin, M. T.; Vauthier, E. C.; Fliszár, S. *Can. J. Chem.* **1985**, *63*, 3226.
(9) Escudero, F.; Mó, O.; Yánez, M. *J. Chem. Soc., Perkin Trans. 2* **1983**, 1735.
(10) Nitrogen atoms contained in aromatic structures exhibit the same behavior as aromatic and ethylenic carbon atoms and carbonyl oxygen. An increase in total electronic population, accompanied by an upfield resonance shift, occurs when the gain in π charge prevails over the concurrent loss in σ electrons. Conversely, nitrogen in alkylamines, nitroalkanes, and isonitriles behaves like typical sp^3 carbon, carbonyl carbon, and dialkyl ether oxygen atoms; any increase in total electronic population translates into a downfield resonance shift when the gain in charge is dictated by that of the σ population.
(11) Bradamante, S.; Pagani, G. A. *J. Chem. Soc., Perkin Trans. 2* **1986**, 1055.
(12) (a) Barchiesi, E.; Bradamante, S. *J. Phys. Org. Chem.* **1990**, *3*, 139. (b) Bradamante, S.; Pagani, G. A. *Pure Appl. Chem.* **1989**, *61*, 709.

0002-7863/92/1514-8634$03.00/0

pulsion and exchange interactions with the others. Thus the density distributions derived from σ and π orbitals are not independent, and their coupling was found very pronounced in some cases.[13] In nitranions, an increase in P_σ^N on deprotonation could induce a partial leakage of σ charge to the σ molecular framework and provoke a concomitant release of π charge to the π-conjugated system. The combined fluxes might produce either an increase or a decrease in the nitrogen total charge (P_T^N), and the observed chemical shift change should somehow reflect the plurality of causes.

The search for relationships between chemical shifts and charges tacitly assumes that the shielding is related to ground-state wave-function properties only. However, NMR chemical shifts are magnetic second-order molecular properties;[14] thus both the isotropic shieldings ($\bar{\sigma}$) and the principal components σ_{ii} [σ_{ii}, i = 1, 2, 3; $\sigma_{11} \leq \sigma_{22} \leq \sigma_{33}$; $\bar{\sigma} = (\sigma_{11} + \sigma_{22} + \sigma_{33})/3$] of the shielding tensor σ also depend on some type of excitation. Each σ_{ii} can be evaluated, in turn, as a sum of diamagnetic and paramagnetic contributions;[15] the former, which induce an upfield shift with respect to the bare nucleus, depend only on the ground-state wave function, while the latter, which cause a downfield shift, explicitly involve excited states of the unperturbed system. The partitioning in diamagnetic and paramagnetic contributions is somewhat arbitrary, but their sums σ_{ii} are observable quantities. Therefore, any attempt to give a firm physical basis to correlations between charges and chemical shifts is doomed from the outset because of excited-state contributions to the latter. Moreover, the anisotropies of the ^{15}N shielding tensors are reckoned[16] to be rather large, particularly for nitrogens contained in aromatic structures. Thus, granted that charge versus chemical shift correlations still retain some empirical utility, it appears that more illuminating relationships should be sought between anisotropies in shielding and anisotropies in charge distribution.

Ultimately, the aim of the present study is to detail the charge density rearrangement occurring upon deprotonation of a number of nitranion precursors and to explore how this empirically affects the measured and computed ^{15}N nuclear magnetic shielding tensors. The format is as follows: section II outlines the computational methods employed, and section III illuminates the observed charge density rearrangement mechanisms using the quantum theory of atoms in molecules (QTAM).[17] Section IV discusses the results of σ tensor computations, while section V illustrates the correlations of ^{15}N σ tensor components with quantities related to charge density distributions. Concluding remarks are given in section VI.

II. Methods

Ab initio computations of pyrrole (**1**), X-aminopyridine (X = 2–4; **2–4**) and their corresponding nitranions (**1a–4a**), and pyridine (**5**) and pyridinium cation (**5c**) (Chart I) were performed at the RHF/6-31G+ level[18] using the Gaussian 88[19] package. The choice of a diffuse basis set was mandatory[18] in order to investigate both **1–4** and their nitranions at the same level. For (**2a–3a**) the two planar conformers with the amino hydrogen on the same (syn) or on the opposite (anti) side with respect

Chart I

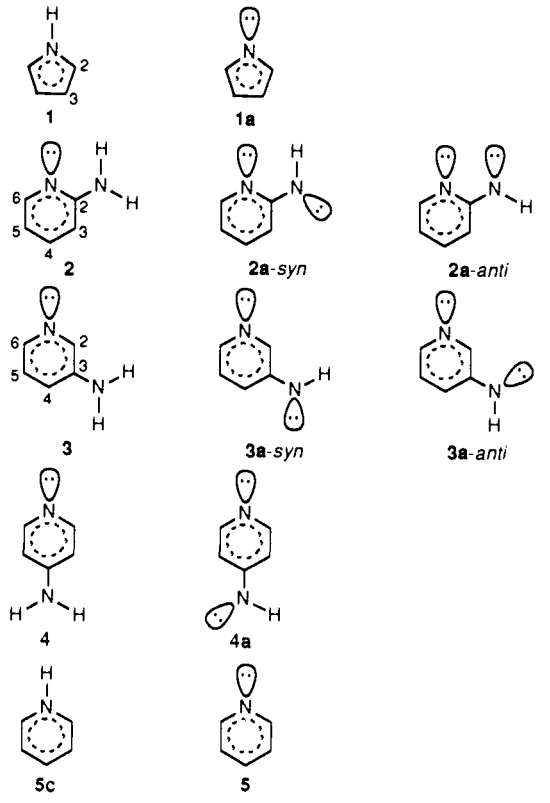

to the pyridine nitrogen were investigated. A full geometrical optimization for all the systems was performed, allowing also for nonplanar conformations. As resulting geometries always turned out to be planar (maximal out of plane nuclear displacements being less than 10^{-3} Å), a σ/π charge separability was allowed. QTAM has been applied to the study of the investigated systems through a topological analysis of the corresponding RHF/6-31G+ charge densities $\rho(\mathbf{r})$. QTAM defines the structure of a molecule, its structural stability, and the properties of its constituent atoms using only information contained in ρ. Within the theory, in fact, the boundaries of atoms in molecules and the networks of bonds which link them (molecular structure) are uniquely determined by the topology of the gradient vector field ($\nabla\rho$) of ρ. The atomic boundaries exhibit a zero-flux in the gradient vector of ρ, thus satisfying the quantum condition for the definition of a subsystem with well-defined properties.[17] The same condition yields a unique disjoint partitioning of a molecule into subsystems (each but in few well-documented situations containing a nucleus[20]), and, as a result, the molecular average of a given observable can be expressed as a sum of subsystem contributions. Each atom in a molecule is therefore characterized by its own set of properties, including charge and energy. The QTAM atomic energies individually obey the virial theorem, and the corresponding atomic charges can be referred to as *virial partitioning* atomic charges. Hence, the determination of net atomic charges does not require an arbitrary partitioning of the charge contributions of given subsets of the basis set, as Mulliken population analysis does. Instead, a numerical integration within a physically defined portion of real space is needed. P_σ and P_π are evaluated by summing the relevant diagonal elements $S_{ii}(\Omega)$

$$S_{ij}(\Omega) = \int_\Omega \phi_i \phi_j \, d\tau$$

$$P_\alpha = \sum_{i \in \alpha} S_{ii}(\Omega) \qquad \alpha = \sigma, \pi$$

of the atomic overlap matrix S (in the ϕ molecular orbital basis representation) for each atomic basin Ω.[21]

(13) (a) Cade, P. E.; Bader, R. F. W.; Pelletier, J. *J. Chem. Phys.* **1971**, *54*, 3517. (b) Bader, R. F. W.; Slee, T. S.; Cremer, D.; Kraka, E. *J. Am. Chem. Soc.* **1983**, *105*, 5061.

(14) (a) Lipscomb, W. N. *MTP Int. Rev. Sci., Ser. 1* **1972**, *1*, 167–196. (b) Kutzelnigg, W. *J. Mol. Struct. (THEOCHEM)* **1989**, *202*, 11–61.

(15) Ramsey, N. F. *Molecular Beams*; Oxford University Press: London and New York, 1956; pp 163 and 207.

(16) Bouman, T. D.; Hansen, A. E. *Int. J. Quantum Chem.* **1989**, *S23*, 381–396 and references therein.

(17) (a) Bader, R. F. W. *Atoms* In *Molecules, A Quantum Theory* (International Series of Monographs on Chemistry); Oxford University Press: Oxford, 1990; No. 22. (b) Bader, R. F. W. *Chem. Rev.* **1991**, *91*, 893–928. (c) Bader, R. F. W.; Essen, H. *J. Chem. Phys.* **1984**, *80*, 1943.

(18) Hehre, W. J.; Radom, L.; Schleyer, P. v. R.; Pople, J. A. *Ab initio Molecular Orbital Theory*; Wiley: New York, 1986 and references therein.

(19) (a) Frisch, M. J.; Head-Gordon, M.; Schlegel, H. B.; Raghavachari, K.; Binkley, J. S.; Gonzalez, C.; Defrees, D. J.; Fox, D. J.; Whiteside, R. A.; Seeger, R.; Melius, C. F.; Baker, J.; Martin, R.; Kahn, L. R.; Stewart, J. J. P.; Fluder, E. M.; Topiol, S.; Pople, J. A. *Gaussian 88*; Gaussian Inc.: Pittsburgh, PA, 1988. (b) A Gaussian 88 modified version for GOULD NP1 computer was used: Barzaghi, M. Unpublished work.

(20) (a) Gatti, C.; Fantucci, P.; Pacchioni, G. *Theor. Chim. Acta* **1987**, *72*, 433. (b) Cao, W. L.; Gatti, C.; MacDougall, P. J.; Bader, R. F. W. *Chem. Phys. Lett.* **1987**, *141*, 380. Cioslowski, J. *J. Phys. Chem.* **1990**, *94*, 5496.

(21) VP charges have been recently criticized (Perrin, C. L. *J. Am. Chem. Soc.* **1991**, *113*, 2865–2868) because of their supposed inability to discriminate between size effects and electronegativity. However, this conclusion seems to be biased by erroneous assumptions or too simplistic approximations in the model calculations adopted: Gatti, C.; Fantucci, P. Submitted to *J. Am. Chem. Soc.*

Table I. Electron Population of Nitrogens and of Their Linked Hydrogens[a]

system	virial partitioning			Mulliken partitioning		
	$(P_T^N)_{VP}$	$(P_\sigma^N)_{VP}$	$(P_\pi^N)_{VP}$	$(P_T^N)_{MP}$	$(P_\sigma^N)_{MP}$	$(P_\pi^N)_{MP}$
1	8.233	6.474	1.758	7.677	6.042	1.635
1a	8.081	6.650	1.430	7.436	6.166	1.270
2 (N-py)	8.086	6.696	1.388	7.396	6.182	1.214
2 (N-am)	8.162	6.304	1.858	7.957	6.104	1.854
2a-*syn* (N-py)	8.115	6.648	1.466	7.446	6.126	1.320
2a-*syn* (N-am)	8.103	6.526	1.576	7.812	6.286	1.526
2a-*anti* (N-py)	8.072	6.654	1.422	7.315	6.061	1.254
2a-*anti* (N-am)	8.054	6.478	1.578	7.756	6.227	1.529
$\mathbf{2a}_{av}$ (N-py)	8.094	6.651	1.444	7.381	6.094	1.287
$\mathbf{2a}_{av}$ (N-am)	8.079	6.502	1.577	7.784	6.257	1.528
3 (N-py)	8.078	6.816	1.262	7.259	6.193	1.066
3 (N-am)	8.156	6.276	1.882	8.061	6.178	1.883
3a-*syn* (N-py)	8.148	6.862	1.282	7.281	6.214	1.067
3a-*syn* (N-am)	8.083	6.452	1.632	7.848	6.254	1.594
3a-*anti* (N-py)	8.151	6.860	1.290	7.288	6.208	1.080
3a-*anti* (N-am)	8.082	6.454	1.628	7.840	6.249	1.591
$\mathbf{3a}_{av}$ (N-py)	8.150	6.861	1.286	7.285	6.211	1.074
$\mathbf{3a}_{av}$ (N-am)	8.083	6.453	1.630	7.844	6.252	1.593
4 (N-py)	8.058	6.700	1.350	7.308	6.126	1.182
4 (N-am)	8.163	6.298	1.864	8.040	6.177	1.863
4a (N-py)	8.091	6.614	1.478	7.435	6.103	1.332
4a (N-am)	8.087	6.494	1.594	7.806	6.263	1.544
5c	8.246	6.614	1.632	7.607	6.111	1.496
5	8.072	6.784	1.288	7.261	6.156	1.106

	$(P_T^H)_{VP}$	$(P_\sigma^H)_{VP}$	$(P_\pi^H)_{VP}$	$(P_T^H)_{MP}$
1 (H-py)	0.578	0.560	0.018	0.549
$\mathbf{2}_{av}$ (H-am)	0.586	0.568	0.018	0.575
$\mathbf{2a}_{av}$ (H-am)	0.749	0.723	0.026	0.742
$\mathbf{3}_{av}$ (H-am)	0.599	0.579	0.020	0.582
$\mathbf{3a}_{av}$ (H-am)	0.788	0.745	0.043	0.756
4 (H-am)	0.596	0.576	0.020	0.579
4a (H-am)	0.783	0.757	0.026	0.752
5c (H-py)	0.517	0.505	0.012	0.484

[a] Electron population are labeled as $(P_\alpha^X)_{YP}$ ($\alpha = \sigma$, π, or T for σ, π, and total $\equiv \sigma + \pi$) electron populations, respectively; X = N, H, or C for nitrogen, hydrogen, or carbon; Y = V or M for virial or Mulliken electron population partitionings). N-py and N-am refer to pyridyl and amino-group nitrogens, respectively. H-py and H-am are the corresponding linked hydrogens. The two planar conformations for **2a** and **3a** are labeled syn or anti whether the remaining amino proton is the one closer to the pyridic nitrogen or not. Populations for each conformer are reported along with their average ($\mathbf{2a}_{av}$ and $\mathbf{3a}_{av}$). For hydrogens only average values are reported for both protonated and deprotonated systems.

Electronic moments other than the monopole (the net charge) may be determined for an atom in a molecule by averaging the corresponding operator over the charge density on Ω. In view of possible correlations with σ tensor components, we computed the components of the traceless quadrupole moment tensor Q, defined as

$$Q_{ij}(\Omega) = -\int_\Omega \rho(3ij - r^2)\,d\tau \qquad i,j = x, y, z$$

where $r = |\mathbf{r}|$. For a spherical distribution, the Q_{ii} are equal to zero, while a negative Q_{ii} value indicates an accumulation of charge in the ii direction at the expense of the direction(s) associated with a positive Q_{jj} component.

The topological properties of $\rho(\mathbf{r})$ and the numerical integration within each atomic basin were performed with the PROAIM[22] package.

The ^{15}N nuclear magnetic shielding tensors σ, along with their principal components σ_{ii}, were computed within the linear response of a single-determinant wave-function approach. The localized orbital–local origin (LORG) method[23] and the RPAC program,[24] suitably interfaced with GAUSSIAN 88,[19] were used.

III. Charge Density Analysis

The numbering of investigated systems, along with the labeling of their constituent atoms, is reported in Chart I. Table I and Table III list the nitrogen, hydrogen, and carbon total and σ and π electron populations of the systems studied, whereas Table II and Table IV show the changes in these quantities for **1–4** and **5c** upon deprotonation. In the latter tables, a minus sign indicates decrease of electron population in nitranions with respect to their neutral precursors, and conversely a plus sign indicates an increase. For the sake of completeness, electron populations are reported for both virial partitioning (VP) and Mulliken partitioning (MP) schemes and are generally labeled as $(P_\alpha^X)_{YP}$ ($\alpha = \sigma$, π, or T, for σ, π, and total $\equiv \sigma + \pi$ electron populations, respectively; X = C, N, or H for carbon, nitrogen, or hydrogen; Y = V or M for virial and Mulliken populations). The corresponding changes upon deprotonation are labeled as $(\Delta P_\alpha^X)_{YP}$.

Table I shows that, within the VP scheme, the **2–4** nitrogen total electron populations are nearly constant for pyridic (N-py) and amino-group (N-am) nitrogens, the latter being some 0.1 electron greater than the former. The σ and π populations clearly discriminate between the two classes of nitrogen. The π-electron populations of amino-group nitrogen are some 0.5 electron greater than the N-py ones and close to a value of 2. The corresponding differences in σ nearly compensate for the reported differences in π populations, thus confirming the well-known[6,8] inverse relationship between σ and π charges in this class of compounds. The MP scheme yields quite different $(P_T^N)_{MP}$ values for the two classes of nitrogens, the N-py ones being some 0.7 electron less than those for N-am. This difference results from a nearly constant σ population and a sharply different π population, even greater than that provided by the VP scheme. The inability of MP to properly describe the inverse relationship between σ and π charges is mostly due, here, to the use of a basis set including diffuse functions.[25] Though VP charges are also basis set dependent (as due to the changes induced in $\rho(\mathbf{r})$ and in its derivatives), they are much more stable against a change in basis set type, provided a high quality of the wave function is maintained. This behavior, which is anticipated by the physical basis on which VP is grounded, was elucidated[26] by comparing VP and MP charges for some typical hydrocarbons and for a series of AH_n hydrides ($n = 1, 2$), using a wide range of basis sets (STO-3G, 3-21G, 6-31G, 6-31G*, 6-31G**, 6-31G**+). Table II indicates that a net decrease in pyrrole, pyridinium cation, and N-am nitrogen electron populations occurs upon deprotonation, as a result of a sharp decrease in π and a lesser increase in σ population. Simple MO considerations could anticipate the opposite trend of σ and π charges. However, the net charge decrease of these nitrogens, which upon deprotonation "own" a σ lone pair, is, at a first sight, a rather surprising result. A closer inspection (at the VP level) of deprotonated nitrogen σ charge increase indicates that a great amount of the charge made available upon deprotonation is transferred to the σ molecular framework. This charge is almost all σ, as the hydrogen π charge represents, in VP scheme, at most the 5% of the hydrogen total charge. Hence, for example, in **4a** the 0.576 σ electron made available, is partitioned into an increase (0.196 e) of N-am σ charge and into comparable σ charge transfers (CT) to the ring (0.199 e) and to the remaining amino-group hydrogen (0.181 e) (see Tables I and II). The π CT to the ring, $\Delta P_\pi^N = -0.270$, is nearly 150% of the σ in this system. In **1a** and **5** the σ (0.384 and 0.335 e, respectively) and the π

(22) Biegler-König, F. W.; Bader, R. F. W.; Tang, T. *J. Comput. Chem.* **1982**, *3*, 317.

(23) (a) Hansen, A. E.; Bouman, T. D. *J. Chem. Phys.* **1985**, *82*, 5035. (b) Bouman, T. D.; Hansen, A. E. *Chem. Phys. Lett.* **1988**, *149*, 510.

(24) Bouman, T. D.; Hansen, A. E. RPAC Version 8.4, revision of Program. No. 556; Quantum Chemistry Program Exchange, Indiana University: Bloomington, IN, 1988.

(25) Due to their spatial extension, diffuse functions of N-am nitrogen are used in the SCF procedure to describe amino-hydrogen electrons. However, the populations of these hydrogens are, in the MP scheme, invariably assigned to N-am, making this atom more charged than it should be. Conversely, N-py nitrogen, which has no hydrogen linked to it, undergoes a decrease in its population as a result of the MP half-and-half partitioning of overlap populations (N-py has two, instead of one, less electronegative atom provided with diffuse basis set, linked to it). These considerations are confirmed by RHF/6-31G results (diffuse functions are left out here). The difference in N-py and N-am MP electron populations is decreased to 0.43 electron, differences in net populations, and in half the overlap populations being 0.282 e (0.375, 6-31G+) and 0.148 e (0.375, 6-31G+), respectively.

(26) Gatti, C. Unpublished work.

Table II. Total, σ, and π Nitrogen Electron Population Changes (ΔP) of **1**–**4** and **5c** upon Deprotonation[a]

system	virial partitioning			Mulliken partitioning		
	$(\Delta P_T^N)_{VP}$	$(\Delta P_\sigma^N)_{VP}$	$(\Delta P_\pi^N)_{VP}$	$(\Delta P_T^N)_{MP}$	$(\Delta P_\sigma^N)_{MP}$	$(\Delta P_\pi^N)_{MP}$
1	−0.152	0.176	−0.328	−0.241	0.124	−0.365
$\mathbf{2}_{av}$ (N-py)	0.008	−0.045	0.056	−0.015	−0.088	0.073
$\mathbf{2}_{av}$ (N-am)	−0.083	0.198	−0.281	−0.173	0.153	−0.326
$\mathbf{3}_{av}$ (N-py)	0.072	0.045	0.024	0.026	0.018	0.008
$\mathbf{3}_{av}$ (N-am)	−0.073	0.177	−0.252	−0.217	0.074	−0.290
4 (N-py)	0.033	−0.086	0.128	0.127	−0.023	0.150
4 (N-am)	−0.076	0.196	−0.270	−0.234	0.086	−0.319
5c	−0.174	0.170	−0.344	−0.346	0.045	−0.390

[a] See the corresponding footnote of Table I for explanation of symbols; a minus (plus) sign indicates decrease (increase) of electron population upon deprotonation. The average changes for the two nitranion conformers are reported for **2** and **3** (see footnote in Table I).

Table III. Carbon Electron Population for the Investigated Systems[a]

system		virial partitioning			Mulliken partitioning		
		$(P_T^C)_{VP}$	$(P_\sigma^C)_{VP}$	$(P_\pi^C)_{VP}$	$(P_T^C)_{MP}$	$(P_\sigma^C)_{MP}$	$(P_\pi^C)_{MP}$
1	C2	5.639	4.642	0.998	6.187	5.100	1.087
	C3	6.018	4.962	1.054	6.186	5.091	1.095
1a	C2	5.705	4.660	1.042	6.326	5.180	1.146
	C3	6.135	4.982	1.154	6.277	5.057	1.219
2	C2	5.106	4.344	0.760	5.853	4.972	0.880
	C3	6.032	4.952	1.080	5.809	4.683	1.126
	C4	5.972	5.084	0.888	6.473	5.571	0.901
	C5	6.037	4.972	1.064	6.133	5.015	1.118
	C6	5.502	4.690	0.810	6.171	5.264	0.907
$\mathbf{2a}_{av}$	C2	5.171	4.435	0.736	6.177	5.315	0.863
	C3	6.088	4.974	1.113	5.861	4.701	1.160
	C4	6.013	5.076	0.932	6.390	5.445	0.945
	C5	6.129	4.914	1.213	6.285	4.966	1.319
	C6	5.508	4.697	0.813	6.106	5.206	0.900
3	C2	5.510	4.590	0.924	6.192	5.135	1.057
	C3	5.591	4.690	0.896	5.650	4.733	0.916
	C4	6.014	4.994	1.018	6.237	5.176	1.061
	C5	6.003	5.046	0.956	6.020	5.041	0.980
	C6	5.526	4.614	0.910	6.351	5.314	1.037
$\mathbf{3a}_{av}$	C2	5.544	4.584	0.958	6.137	5.022	1.115
	C3	5.552	4.747	0.802	6.191	5.359	0.833
	C4	6.088	4.983	1.104	6.108	4.939	1.169
	C5	6.034	5.061	0.973	5.956	4.961	0.995
	C6	5.628	4.555	1.069	6.463	5.239	1.225
4	C2	5.511	4.696	0.812	6.368	5.455	0.913
	C3	6.043	4.954	1.088	5.745	4.605	1.140
	C4	5.558	4.728	0.832	6.190	5.341	0.849
4a[b]	C2	5.592	4.735	0.857	6.330	5.389	0.941
	C3	6.109	4.965	1.142	5.686	4.457	1.229
	C4	5.505	4.740	0.766	6.699	5.915	0.784
5c	C2	5.494	4.710	0.784	6.123	5.258	0.865
	C3	5.949	4.995	0.954	5.968	4.977	0.991
	C4	5.930	5.140	0.782	6.318	5.527	0.791
5	C2	5.515	4.677	0.838	6.296	5.345	0.951
	C3	6.023	5.033	0.990	5.955	4.929	1.026
	C4	5.993	5.073	0.920	6.438	5.495	0.943

[a] See footnote *a* in Table I for explanation of symbols. The average values only ($\mathbf{2a}_{av}$, $\mathbf{3a}_{av}$) are listed for the two planar conformers of **2a** and **3a**. Carbon atoms are labeled according to Chart I. [b] For the sake of comparison with **2a** and **3a**, populations are reported supposing free rotation around the C_4–N_{am} bond.

Table IV. Total, σ, and π Carbon Electron Population Changes (ΔP) of **1**–**4** and **5c** upon Deprotonation[a,b]

system		virial partitioning			Mulliken partitioning		
		$(\Delta P_T^C)_{VP}$	$(\Delta P_\sigma^C)_{VP}$	$(\Delta P_\pi^C)_{VP}$	$(\Delta P_T^C)_{MP}$	$(\Delta P_\sigma^C)_{MP}$	$(\Delta P_\pi^C)_{MP}$
1	C2	0.066	0.018	0.044	0.139	0.080	0.059
	C3	0.117	0.020	0.100	0.091	−0.034	0.124
$\mathbf{2}_{av}$	C2	0.065	0.091	−0.024	0.324	0.343	−0.017
	C3	0.056	0.022	0.033	0.052	0.018	0.034
	C4	0.041	−0.008	0.044	−0.083	−0.126	0.044
	C5	0.092	−0.058	0.149	0.152	−0.049	0.201
	C6	0.006	0.007	0.003	−0.065	−0.058	−0.007
$\mathbf{3}_{av}$	C2	0.034	−0.006	0.034	−0.055	−0.113	0.058
	C3	−0.039	0.057	−0.094	0.541	0.626	−0.083
	C4	0.074	−0.011	0.086	−0.129	−0.237	0.108
	C5	0.031	0.015	0.017	−0.064	−0.080	0.015
	C6	0.102	−0.059	0.159	0.112	−0.075	0.188
4[c]	C2	0.081	0.039	0.045	−0.039	−0.067	0.028
	C3	0.066	0.011	0.054	−0.059	−0.148	0.089
	C4	−0.053	0.012	−0.066	0.509	0.574	−0.065
5c	C2	0.021	−0.033	0.054	0.173	0.087	0.086
	C3	0.074	0.038	0.036	−0.013	−0.048	0.035
	C4	0.063	−0.067	0.138	0.120	−0.032	0.152

[a] See the corresponding note of Table II. [b] Carbon atoms are labeled according to Chart I. [c] See footnote *b* of Table III.

(0.346 and 0.356 e, respectively, including the hydrogen π charge) CTs to the ring are similar and significantly higher than the nitrogen σ charge increase.[27] Overall, it can be said that the σ-charge increase upon deprotonation pushes away an even greater amount of π charge. This latter, unlike the σ charge, can be efficiently delocalized and concentrated in the ring nuclei only, through the π framework.

The resulting changes in π-electron populations along the five- or six-membered rings (see also Tables III and IV) can be easily understood in terms of resonance structure stability considerations. So, in **2a** for example, the greatest change in carbon π-electron population is for C_5 owing to the greater stability of the quinoid-like resonance structure. Similar considerations easily explain the changes observed for the other compounds.

The charge density rearrangement mechanism, which has been so far discussed from an *integral* (P_α^X) point of view, can be investigated in a more pictorial and *local* way by studying the changes occurring in $\rho(\mathbf{r})$ upon deprotonation. To this end, there follows a brief outline of the chemical insight provided by the topological study of ρ.

The topological properties of a scalar field such as ρ and its Laplacian $\nabla^2\rho$ are summarized in terms of their critical points $\mathbf{r}_c$—the points where $\nabla\rho$ and $\nabla(\nabla^2\rho)$ are equal to zero. Critical points are classified according to their type (m, n) by stating their rank m and signature n. The rank is equal to the number of nonzero eigenvalues of the Hessian matrix of ρ or $\nabla^2\rho$ at $\mathbf{r}_c$. The signature equals the algebraic sum of the signs of the eigenvalues (or principal curvatures) of ρ or $\nabla^2\rho$ at $\mathbf{r}_c$. An atomic interaction is characterized by a line linking two nuclei along which the charge density ρ is a maximum with respect to any lateral displacement. If such a line is present in a minimum energy geometry, the line is referred to as a *bond path*, and the two atoms are said to be bonded to one another. The local properties of ρ at the *bond critical point* (bcp: the point of minimum charge density along the bond path) give[17c] a concise description of the particular type of atomic interaction occurring between bonded atoms. The bcp is a $(3, -1)$ critical point with one positive curvature (λ_3) and two negative curvatures (λ_1 and λ_2, $\lambda_1 \leq \lambda_2$). The positive curvature is associated with an eigenvector of the Hessian matrix of ρ at $\mathbf{r}_c$ pointing along the bond direction, while the two negative curvatures are associated with eigenvectors perpendicular to the bond path. The value of the charge density at the bcp, ρ_b, serves[13b] as a measure of the bond order n. The two negative curvatures of a bond critical point define the bond *ellipticity* ϵ, a measure of the extent to which charge is preferentially accumulated in a given plane.[17] This is defined as $\epsilon = (\lambda_1/\lambda_2) - 1$. The axis associated with λ_2 defines the *major axis* of the elliptical contour

(27) Note that no net transfer of the made available σ charge is possible to the π framework as both protonated and deprotonated systems have the same number of π MOs (i.e., 3 for **1** and **5**, and 4 for **2**–**4**).

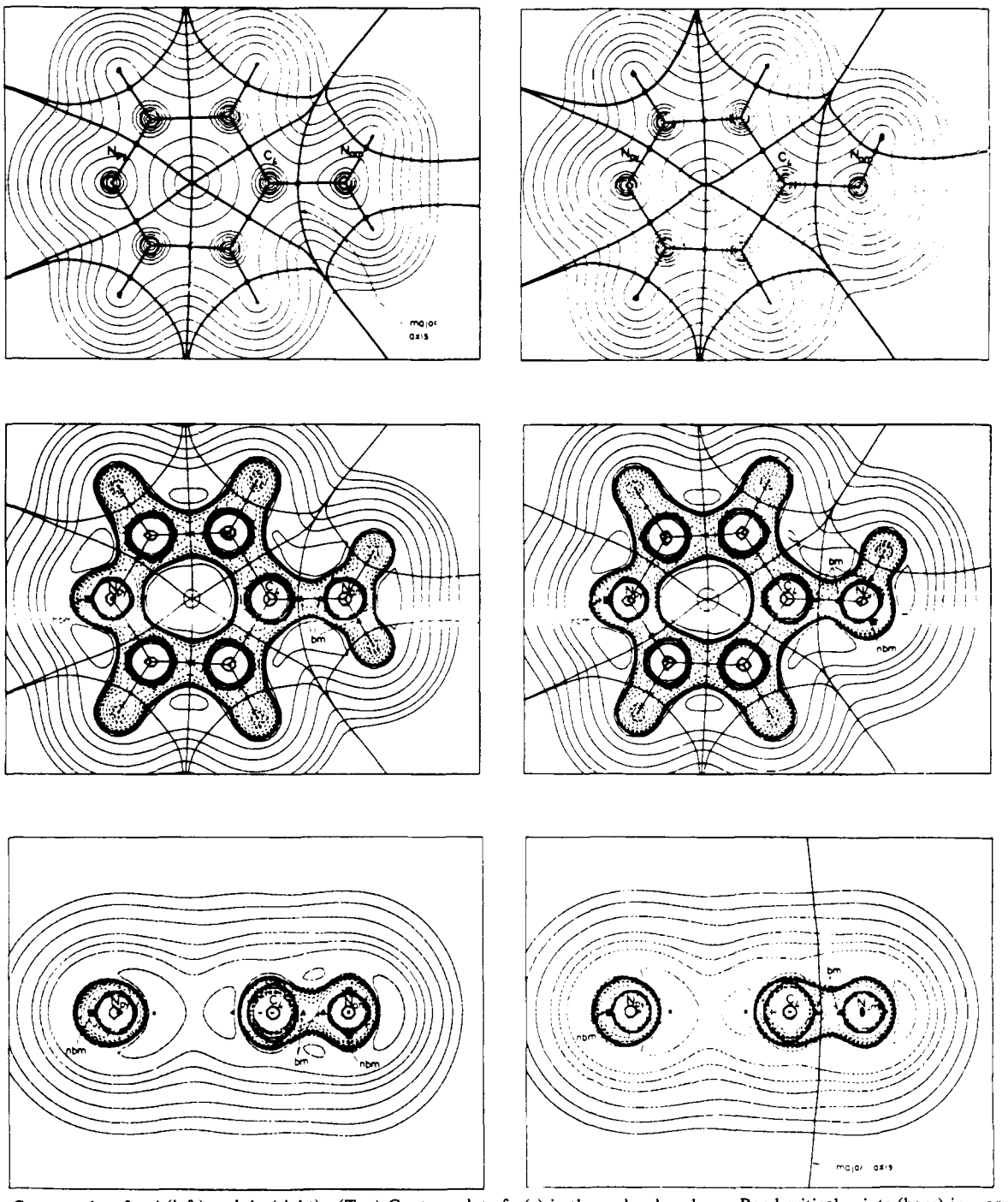

Figure 1. Contour plots for **4** (left) and **4a** (right). (Top) Contour plot of $\rho(\mathbf{r})$ in the molecular plane. Bond critical points (bcps) in ρ are denoted by ●. The pair of $\nabla\rho$ trajectories which originate (bond paths) or terminate at bcps are superimposed on the contour maps. These trajectories define the molecular structure and the partitioning of space into atomic subspaces. (Middle) Contour plot of $\nabla^2\rho(\mathbf{r})$ in the molecular plane. Dashed contours denote negative, solid contours positive values of $\nabla^2\rho$, respectively. Bonded maxima (bm) in $-\nabla^2\rho$ are denoted by ▲ and nonbonded maxima (nbm) by ■. (Bottom) Contour plot of $\nabla^2\rho(\mathbf{r})$ in a plane perpendicular to the molecular plane and containing N-py and N-am. The major axis of C_4–N_{am} bond, which lies in the molecular plane for **4** (top, left), is perpendicular to the same plane in **4a**; upon deprotonation, the π conjugation between the amino group and the heterocyclic ring has been "switched on".

of ρ about the bond axis. For the CC bond in ethane, λ_1 and λ_2 are obviously degenerate and ϵ is zero; in conjugated systems (e.g., *trans*-1,3-butadiene), the major axes of the CC bonds are all parallel[13b] and point in the direction of the maximum in π distribution in the usual MO theory.

The topology of another scalar field related to the charge density, namely, its Laplacian $\nabla^2\rho$, allows[17c,28] one to recover the chemical model of the localized bonded and nonbonded pairs and in general to characterize local concentrations ($\nabla^2\rho < 0$) and depletions ($\nabla^2\rho > 0$) of electronic charge. The Laplacian distribution of ρ for a free atom reflects the quantum shell structure by exhibiting the corresponding number of alternating pairs of shells of charge concentration and charge depletion (the inner shell of each pair always being the region of charge concentration). Upon bonding, local maxima in $-\nabla^2\rho$ (3, −3) critical points are formed in the valence shell of charge concentration (VSCC). The number of resulting *bonded* and *nonbonded* maxima (hereinafter denoted as bm and nbm, respectively) are found to be in agreement with the Lewis model of localized electron pairs. Hence each carbon in ethylene possesses three bonded concentrations in agreement with the sp^2 MO picture, while each carbon in ethane

(28) Bader, R. F. W.; MacDougall, P. J.; Lau, C. D. H. *J. Am. Chem. Soc.* **1984**, *106*, 1594.

Table V. Changes in $-\nabla^2_\rho$ Maxima Properties for **1**, **4**, and **5c** upon Deprotonation[a,b]

system	bond	kind[c]	R_x[d]	loc.[e]	ρ	$-\nabla^2_\rho$
1 (**1a**)	N	nbm	0.76 (0.74)	⊥ (∥)	0.49 (0.58)	1.887 (3.127)
1 (**1a**)	$\bar{N}$–C	bm	0.80 (0.80)	∥ (∥)	0.48 (0.47)	1.744 (1.726)
1 (**1a**)	N–$\bar{C}$	bm	1.03 (0.99)	∥ (∥)	0.28 (0.31)	0.699 (0.894)
1	$\bar{N}$–H	bm	0.80	∥	0.48	1.800
4 (**4a**)	(N_{am})	nbm	0.75 (0.75)	⊥ (∥)	0.53 (0.55)	2.433 (2.696)
4 (**4a**)	($\bar{N}_{am}$)–C	bm	0.82 (0.82)	∥ (∥)	0.45 (0.45)	1.444 (1.493)
4 (**4a**)	(N_{am})–$\bar{C}$	bm	1.00 (0.95)	∥ (∥)	0.29 (0.34)	0.844 (1.149)
4 (**4a**)	($\bar{N}_{am}$)–H	bm	0.81 (0.82)	∥ (∥)	0.47 (0.43)	1.617 (1.427)
4 (**4a**)	($\bar{N}_{py}$)–C	bm	0.80 (0.81)	∥ (∥)	0.48 (0.46)	1.787 (1.630)
4 (**4a**)	(N_{py})–$\bar{C}$	bm	0.98 (0.97)	∥ (∥)	0.33 (0.32)	1.015 (1.012)
4 (**4a**)	(N_{py})	nbm	0.73 (0.74)	∥ (∥)	0.62 (0.58)	3.531 (3.120)
5c (**5**)	N	nbm	0.78 (0.73)	⊥ (∥)	0.45 (0.63)	1.464 (3.700)
5c (**5**)	$\bar{N}$–C	bm	0.79 (0.79)	∥ (∥)	0.50 (0.49)	1.941 (1.894)
5c (**5**)	N–$\bar{C}$	bm	1.02 (0.98)	∥ (∥)	0.30 (0.33)	0.817 (0.987)
5c	$\bar{N}$–H	bm	0.79	∥	0.51	2.095

[a] The values for the deprotonated forms are reported in parentheses. [b] All quantities in atomic units (au). [c] nbm = nonbonded maximum; bm = bonded maximum. [d] Critical point distance to the underlined nucleus in column 2. [e] (⊥) the maximum is located R_x au above (or below) the nucleus; (∥) the maximum lies R_x au far from the nucleus, in the molecular plane.

exhibits four bonded concentrations corresponding to the sp^3 hybridization model.

In our case ρ and $\nabla^2\rho$ topologies should shed light on the extent of N-am participation to the π-delocalized system in **2**–**4** and on the changes caused by deprotonation. Figure 1 shows ρ and $\nabla^2\rho$ contour lines in the molecular plane of **4** and **4a** ($\nabla^2\rho$ is also displayed in a plane perpendicular to the molecular plane and containing N-py and N-am). Table V reports the changes in $-\nabla^2\rho$ maxima properties for **1**, **4**, and **5c** upon deprotonation. Figure 1 and Table V indicate that N-am in **4** has two nbm in $-\nabla^2\rho$ in a plane perpendicular to the molecular plane, located at some 0.75 au above and below the N-am nucleus. These out-of-plane nbm maxima translate into a single more pronounced in-plane nbm in **4a**, corresponding to the N-am lone pair.[29] The out-of-plane locations of nbms in **4** indicate that here the π conjugation between the amino group and the heterocyclic ring is partly *switched off*. This is also supported (Figure 1) by the fact that the major axis of the C–N_{am} bond (ϵ = 0.058) lies in the molecular plane, i.e., perpendicular to all the ring major axes. Upon deprotonation, the C–N_{am} bond ellipticity (ϵ = 0.067) does not change significantly in value, but the bond major axis aligns with the ring axes (Figure 1), thereby indicating that the π conjugation has now been *switched on*. Accordingly, the C–N_{am} bond distance decreases from 1.371 to 1.322 Å and the bond order n rises from 1.30 to 1.64,[30] as a consequence of the increase of ρ at bcp (from 0.293 to 0.340 au). The bcp moves toward the N-am nucleus, confirming the lowering of its electron population, and the bm $-\nabla^2\rho$ values of the C–N_{am} bond significantly increase in value. A behavior similar to that observed in **4** is found for N-am in **2** and **3** and for pyridic nitrogen in **1** and **5c** (see Table V). Of particular interest are the changes occurring by deprotonating **1** and **5c**. Although the nitrogen can, for both protonated and deprotonated molecules, supply to the π-delocalized system a number (2 in **1**, **1a**; 1 in **5c**, **5**) of electrons such as to fulfill the $4n + 2$ rule, large differences are found in the extent of π delocalization. The nitrogen in **1** and **5c** exhibits $-\nabla^2\rho$ nbms, which relate to unshared π electrons above and below the molecular plane. Correspondingly, the C–N bond ellipticity is very small in **1** (ϵ = 0.03), and even it relates to a preferential accumulation of charge in the molecular plane in **5c** (ϵ = 0.13). By deprotonating **5c** the C–N bond major axis aligns with the ring major axes, and the charge at the C–N bcp rises significantly with a corresponding bond order increase from 1.340 (**5c**) to 1.516 (**5**). In the case of **1**, deprotonation increases noticeably both the C–N bond order (**1**, n = 1.226; **1a**, n = 1.408) and ellipticity (**1**, ϵ = 0.03; **1a**, ϵ = 0.13). It is remarkable, here, that the bond-order changes do not translate in appreciable bond length changes (from 1.373 to 1.360 Å in **1** and from 1.344 to 1.333 in **5c**). Indeed the former are a consequence of important changes in the nature of the C–N bond which becomes significantly less ionic upon deprotonation. In fact,[17c] the absolute value of the Laplacian is doubled at the C–N bcp, mainly as a result of a near-halving of the positive curvature λ_3. This observation emphasizes the importance[13b] of relating ρ_b value changes, rather than bond lengths, to bond order changes. Many

Table VI. Effect of Basis Set, Geometry, Localization Procedure, and Gauge Choice on the Calculated ^{15}N Isotropic Chemical Shift of Pyrrole (**1**) and Pyrrole Nitranion (**1a**)

basis set	geometry	π loc.[a]	gauge[b]	δ(**1**)[c]	δ(**1a**)[c]	$\Delta\delta$
6-31G+	6-31G+[d]	no	L	151.9	323.2	171.3
		no	FL	154.5	324.0	169.6
		yes	L	145.9	319.2	173.3
		yes	FL	158.7	327.9	169.2
6-31G*	6-31G+[d]	no	L	122.9	248.1	125.2
		no	FL	130.5	255.4	124.9
		yes	L	124.3	255.1	130.8
		yes	FL	130.2	261.0	130.8
6-31G*	6-31G*[d]	no	L	110.7	223.3	112.6
		no	FL	120.9	233.4	112.6
		yes	L	112.1	230.4	118.3
		yes	FL	120.6	239.1	118.6
exptl				154.1	239.0	84.9

[a] (yes) core, σ, and π valence orbitals were separately localized; (no) only core and σ valence orbitals were separately localized. [b] Choice of individual gauge of (localized) orbitals according to LORG (L) or FULL LORG (FL) criterion (see text). [c] Calculated chemical shift δ relative to $\bar{\sigma}(NH_3)$ with the corresponding basis set and geometry choices. The LORG $\bar{\sigma}(NH_3)$ values, with respect to the bare nucleus, are (ppm) 281.16, 260.24, and 250.36 for the 6-31G+//6-31G+, 6-31G*//6-31G+, and 6-31G*//6-31G* cases, respectively. The corresponding FULL LORG values are (ppm) 331.55, 323.29, and 315.79. [d] Geometry data (bond lengths in Å, angles in degrees): **1** (**1a**) 6-31G+ geometry: C–N 1.373 (1.360), C2–C3 1.366 (1.398), C3–C4 1.431 (1.417), N–H1 0.990, C2–H2 1.067 (1.072), C2–H3 1.068 (1.073), C2–N–C5 109.6 (106.1), N–C2–C3 107.9 (111.2), N–C2–H2 121.5 (120.8), C2–C3–H3 126.0 (127.0). **1** (**1a**) 6-31G* geometry: C–N 1.363 (1.344), C2–C3 1.358 (1.387), C3–C4 1.427 (1.412), N–H1 0.992, C2–H2 1.070 (1.080), C2–H3 1.071 (1.078), C2–N–C5 109.5 (104.9), N–C2–C3 108.2 (112.5), N–C2–H2 121.1 (120.4), C2–C3–H3 126.0 (127.3).

(29) A study on carbenes [(a) MacDougall, P. J.; Bader, R. F. W. *Can. J. Chem.* **1986**, *64*, 1496. (b) Gatti, C.; MacDougall, P. J.; Bader, R. F. W. *J. Chem. Phys.* **1988**, *88*, 3792] has shown that the local VSCC maxima mimic not only the model of localized bonded and nonbonded pairs but also reflect the presence of local concentrations of unpaired electrons. A single nbm is thus found on the C_{2v} axis in the VSCC of carbon in singlet methylene, while the triplet state exhibits two smaller nbm in the plane perpendicular to the plane of the nuclei. Instead, the two out-of-plane nbms in **4** are due to the lack of participation of the (p_z)-nitrogen lone pair to the C–N bond.

(30) Bond orders n for C–N bonds were computed according to

$$n = \exp\{A[\rho_b(CN) - B]\}$$

where ρ_b(CN) is the value of ρ in au at the CN bcp and with A and B equal to 4.9323 and −0.2396, respectively. The values of A and B parameters were determined by a least-squares method, assigning bond order values of 1, 2, and 3 to methylamine, methylenimmine, and hydrogen cyanide, respectively, and using the corresponding RHF/6-31G+ optimized geometry ρ_b(CN) data.

cases which exhibit quite different chemical behavior (but are not discriminated by bond length) may be covered[31] this way.

IV. Nuclear Magnetic and Electron Atomic Population Anisotropies

Table VI reports the results of preliminary calculations on **1** and **1a** for the ^{15}N isotropic chemical shifts δ. The combined effects on δ of localization procedure, basis set, geometry, and gauge choice have been scrutinized in order to select the most suitable level of computation for the whole set of our systems. Concerning localization, the random-phase approximation theory (on which RPAC program is based) is indeed invariant[16,23] to unitary transformations within the occupied orbital space. For a finite basis set, however, different localization schemes affect the computed σ tensor through the assignment of local origins to the orbitals. A separate localization of core, σ, and π valence orbitals did not introduce unphysical loss of nuclear site symmetry in the computed ^{13}C δ for **1** and **1a**. However, the results obtained without a previous π localization were always closer to experiment. Hence we used canonical π orbitals in the computations for the whole set of compounds; undesired differences in the computed $\bar{\sigma}$ for equivalent nuclei (possibly induced by the choice of a particular Kekulé-type bond structure in the π localization step) were also a priori avoided this way. The other computational conditions were set according to the following considerations. Focussing on the experimental chemical shift change $\Delta\delta$ upon deprotonation ($\Delta\delta = \delta(\mathbf{1a}) - \delta(\mathbf{1}) = 84.9$ ppm), we note that the computed $\Delta\delta$ are always overestimated. This generally results from a fairly accurate prediction for $\delta(\mathbf{1a})$ and an underestimate of $\delta(\mathbf{1})$. The opposite is true (with **1** and **1a** interchanged) for RPAC/6-31G+//6-31G+ computations (RPAC with 6-31G+ basis set at the RHF/6-31G+ geometry), whose selection can, however, be discarded owing to the worst $\Delta\delta$ estimate among the computational levels considered. Negligible changes in $\Delta\delta$ have been obtained using the FULL LORG, instead of the more usual LORG criterion, for the choice of the individual gauge of orbitals.[32] Thus the latter option has been adopted. The use of RHF/6-31G* geometry gives the best agreement between experimental and computed RPAC/6-31G* $\Delta\delta$s. However, the deviation of RPAC/6-31G*//6-31G* $\Delta\delta$ from experiment (27 ppm) is still rather large and comparable to that for RPAC/6-31G*//6-31G+ (40 ppm). These considerations, together with large shift dependence on sample phase[16,33] common in molecules containing lone pairs (**1a**) or unpaired electrons (**1**; see section 3), suggest that no conclusive statements about the choice of an "optimum" geometry can be made. It has also been recently hypothesized,[16] in a study of σ tensors of pyridine and heterocyclic azines, that the major source of discrepancy between experiment and theory is due, there, to an incorrect description of the lone pair contributions. It appears[16] that the latter may well require a treatment similar to that used for molecular anions. RPAC/6-31G+//6-31G+ results seem to rule out this hypothesis, at least in the case of our compounds. Indeed, the use of both polarization and diffuse functions would be the best choice for the description of lone pairs (or $n \rightarrow \pi^*$ excitations), but this would require much more extensive computations. In conclusion, the RPAC/LORG/6-31G*//6-31G+ level, with separate localizations of core and σ valence orbitals, was selected. This choice looks like a fair compromise between accuracy and computational expense. Moreover, it allows one to use the same reference geometries in charge density and chemical shift analysis.

Table VII. Experimental Versus Computed Results for the ^{15}N Isotropic Chemical Shifts δ and Their Changes $\Delta\delta$ upon Deprotonation

system (nucleus)	$\bar{\sigma}$(calcd)[a]	δ(calcd)[b]	δ(exptl)[c]	$\Delta\delta$(calcd)[d]	$\Delta\delta$(exptl)[d]
1	137.4	122.9	154.1		
1a	12.2	248.1	239.0	125.2	84.9
2 (N-py)	13.7	246.5	265.7		
2a$_{av}$ (N-py)[e]	25.2	235.0	246.0	−11.5	−19.7
3 (N-py)	−78.5	338.7	315.5		
3a$_{av}$ (N-py)[e]	−76.4	336.6	310.2	−2.1	−5.3
4 (N-py)	−12.8	273.0	275.0		
4a (N-py)	62.7	197.5	234.3	−75.5	−40.7
5c	94.2	166.0	214.6		
5	−62.2	322.4	316.7	156.4	102.1
2 (N-am)	202.4	57.8	72.8		
2a$_{av}$ (N-am)[e]	100.4	159.8	146.5	102.0	73.7
3 (N-am)	218.9	41.3	58.6		
3a$_{av}$ (N-am)[e]	123.1	137.1	122.3	95.8	63.7
4 (N-am)	206.6	53.6	67.8		
4a (N-am)	98.6	161.6	150.0	108.0	82.2

[a] LORG calculations in 6-31G* basis on 6-31G+ geometries. $\bar{\sigma}$ isotropic shieldings in ppm, relative to bare nucleus ($\bar{\sigma} = (\sigma_{11} + \sigma_{22} + \sigma_{33})/3$). [b] Calculated chemical shift δ relative to $\bar{\sigma}$(calcd, NH_3) = 260.24 ppm (see Table VI). [c] **1**–**4**, ref 12a; **5**, ref 46; **5c**, ref 47, relative to liquid NH_3 (0.0 ppm), 380.23 ppm from neat nitromethane. [d] Positive (negative) values represent downfield (upfield) shifts upon deprotonation. [e] The average value for the two conformers (syn or anti) is reported.

Table VII compares experimental versus theoretical δ and $\Delta\delta$ values, for **1**–**5c** systems. The agreement is generally fair, differences in δ not exceeding 50 ppm and being on average 21 ppm for protonated and 16 ppm for deprotonated systems (absolute values). $\Delta\delta$ values are reproduced less well, the maximum discrepancy being 54.3 ppm (for **5** minus **5c**) and the average absolute difference amounting to 28 ppm. These data suggest that environment can affect protonated and deprotonated systems differently. We also note that, for nitrogens undergoing deprotonation, the paramagnetic contribution is systematically overestimated for deprotonated systems (**1a**, **5**, and N-am in **2a**, **3a**, and **4a**) and underestimated for protonated systems. Instead, the same contribution is, for N-py, underestimated in ortho- and para-substituted pyridines (both protonated and deprotonated forms), the opposite being true for the meta derivative.

Our results compare very well with recent IGLO[34,35] and LORG computations[16,36] on a number of six-membered aromatic nitrogen heterocycles. There[16] the average absolute difference in δ values, with respect to experiment, was 38.5 (LORG) and 41.3 ppm (IGLO), using experimental geometries and a basis set of a slightly better quality than ours.

Table VIII displays the values of the principal components of the ^{15}N shielding tensor σ, together with their associated directions. The most shielded direction is always perpendicular to the ring, except for the case of N-am in protonated **2**–**4** systems whose major axis lies in the molecular plane. However, these nitrogens are characterized by small anisotropies $\gamma = \sigma_{33} - (\sigma_{11} + \sigma_{22})/2$ and by an average shielding in the molecular plane, $\bar{\sigma}_{mp}$, nearly equal to the out-of-plane shielding. Deprotonated nitrogens show greater anisotropies than protonated ones (average γ values being 280.4 and 112.2 ppm, respectively) owing to strongly enhanced paramagnetic contributions in the molecular plane. Indeed, the presence of the nitrogen lone pair in the deprotonated form induces a big magnetic moment generated by the $n \rightarrow \pi^*$ excitation. Hence $\bar{\sigma}_{mp}$ values are drastically lowered in protonated forms; average $\bar{\sigma}_{mp}$ values are 147 ppm and −39 ppm for protonated and deprotonated nitrogen atoms, respectively. The anisotropies of nitrogens, like N-py in **2**–**4** and **2a**–**4a**, which do not undergo deprotonation but are inserted in an aromatic system and are conjugatively linked to nitrogens (N-am) undergoing deprotonation

(31) Wiberg, K. B.; Bader, R. F. W.; Lau, C. D. H. *J. Am. Chem. Soc.* **1987**, *109*, 985. (b) Gatti, C.; Barzaghi, M.; Simonetta, M. *J. Am. Chem. Soc.* **1985**, *107*, 878. (c) Gatti, C.; Barzaghi, M.; Bonati, L.; Pitea, D. *Quantum Chemistry—Basic Aspects, Actual Trends*, (Carbó Ed. Studies in Physical and Theoretical Chemistry); Elsevier: New York, 1989; Vol 62, p 401.

(32) In the LORG procedure the local gauge origin is placed on the closest nucleus if the orbital centroid lies closer to it than a fixed threshold (we used 0.95 Å), while in the FULL LORG procedure the local origin always coincides with the orbital centroid.

(33) Large shifts are observed in going from gas phase to condensed phase and from solvent to solvent in such systems.

(34) (a) Kutzelnigg, W. *Isr. J. Chem.* **1980**, *19*, 193. (b) Schindler, M.; Kutzelnigg, W. *J. Chem. Phys.* **1982**, *76*, 1919. (c) Kutzelnigg, W.; Fleischer, U.; Schindler, M. *NMR: Basic Princ. Progr.* **1990**, *23*, 165–262.

(35) IGLO and LORG methods are closely related; see: Facelli, J. C.; Grant, D. M.; Bouman, T. D.; Hansen, A. E. *J. Comput. Chem.* **1990**, *11*, 32–44.

(36) Schindler, M. *Magn. Reson. Chem.* **1988**, *26*, 394.

Table VIII. Calculated Principal Components of the Nitrogen Traceless Charge Density Quadrupole Moment Tensor **Q** and of the ^{15}N Shielding Tensor σ for the Investigated Systems

system (nucleus)	$(\bar{Q}_{mp})^a$	$(Q_{op})^a$	$\sigma_{33}{}^b$	$\sigma_{22}{}^b$	$\sigma_{11}{}^b$	$(\bar{\sigma}_{mp})^c$	γ^d
1	1.42	−2.84	219.6 (⊥)	127.3	65.1	96.2	123.4
1a	1.03	−2.05	262.3 (⊥)	−50.3	−175.4	−112.9	375.2
2 (N-py)	0.91	−1.81	290.7 (⊥)	−56.2	−193.3	−124.8	415.4
2a$_{av}$(N-py)^e	1.10	−2.19	264.6 (⊥)	−39.9	−149.0	−94.5	359.1
3 (N-py)	0.59	−1.18	312.3 (⊥)	145.5	−402.2	−273.9	586.2
3a$_{av}$ (N-py)^e	0.58	−1.16	301.0 (⊥)	−151.3	−378.8	−265.1	566.1
4 (N-py)	0.85	−1.70	312.9 (⊥)	−96.5	−254.7	−175.6	488.4
4a (N-py)	1.14	−2.28	301.8 (⊥)	−22.7	−91.0	−56.9	358.7
5c	1.11	−2.21	257.3 (⊥)	71.9	−46.8	12.6	244.8
5	0.69	−1.37	313.1 (⊥)	−137.1	−362.6	−249.9	562.9
2 (N-am)	1.85	−3.69	251.9	202.9 (⊥)	152.5	202.2	74.2
2a$_{av}$ (N-am)^e	1.62	−3.24	198.2 (⊥)	110.0	−6.9	51.6	146.6
3 (N-am)	1.89	−3.79	254.7	214.9 (⊥)	187.2	221.0	53.7
3a$_{av}$ (N-am)^e	1.74	−3.48	219.3 (⊥)	108.4	41.6	75.0	144.3
4 (N-am)	1.85	−3.70	249.8	210.4 (⊥)	159.7	204.8	64.8
4a (N-am)	1.65	−3.29	213.9 (⊥)	85.2	−3.3	41.0	173.0

^{a}A negative Q_{ii} value indicates accumulation of charge in the ii direction at the expense of the direction(s) associated with a positive Q_{jj} component (see text). $\bar{Q}_{mp}$ is the average value of the principal components with associated eigenvectors in the molecular plane, while Q_{op} is the value of the component whose eigenvector is perpendicular to the molecular plane. Values in au, RHF/631G+//6-31G+ wave function. ^{b}Shielding tensor principal components are ordered in decreasing value (from most shielded to least shielded direction) as $\sigma_{33} \geq \sigma_{22} \geq \sigma_{11}$. All values are absolute, i.e., ppm relative to bare nucleus. A (⊥) sign denotes that the corresponding eigenvector is perpendicular to the molecular plane. $^c\sigma$ average value for the two components in the molecular plane. ^{d}Anisotropy $\gamma = \sigma_{33} - (\sigma_{22} + \sigma_{11})/2$. ^{e}The average value for the two conformers (syn and anti) is reported.

ation, are very high (462 ppm, on average) and slightly greater in protonated than in deprotonated forms. This result derives from a lowering of paramagnetic contributions to $\bar{\sigma}_{mp}$ in deprotonated forms; the importance of the nitrogen lone pair in these latter decreases (compare, e.g., the $-\nabla^2\rho$ values for the nonbonded maximum concentration of N-py in **4** and **4a**; Table V) and so does the related n → π* excitation.

The quadrupole moment tensor **Q** provides insights into the anisotropies of atomic charge distributions. The value of the component perpendicular to the ring (Q_{op}) and the average value of the two principal components[37] associated with the molecular plane directions ($\bar{Q}_{mp}$) are reported in Table VIII for nitrogens. Q_{op}'s are negative indicating that charge is in any case accumulated in the out-of-plane direction and depleted in the molecular plane, with respect to a spherically symmetric distribution. Meanwhile, the investigated systems differ in the *extent* of the out-of-plane accumulation. For nitrogen undergoing deprotonation, the out-of-plane accumulation is greater in the protonated than in the deprotonated forms, in agreement with both the reported mechanisms of deprotonation induced P_π^N and P_σ^N variations and the related changes in the location of the $-\nabla^2\rho$ nonbonded maxima. Conversely, in the case of N-py the out-of-plane charge accumulation is enhanced in deprotonated systems for *o*- and *p*-aminopyridines, the opposite being true for meta derivatives. The observed trends in Q_{op} values of protonated and deprotonated forms nicely parallel the trends in γ values discussed above, with lower γ corresponding to enhanced charge accumulations in the out-of-plane direction. Correlations between anisotropies in charge distribution and shielding tensor components, involving not only individual protonated/deprotonated pairs, but the whole set of compounds, are deferred to the next section.

V. Linear Correlations

Linear correlations were obtained by a standard least-squares method.[38] A full error analysis was carried out yielding standard error on regression parameters and several measures of goodness-of-fit (correlation coefficient *r*, standard error for unit weight,[39] and Hamilton's *R* factor[40]). The significance of regression parameters was checked using Student's *t*-test.[38] Table IX collects the results of correlations relating quantities derived from charge density distributions with quantities associated to nuclear magnetic shielding tensors. A thorough caveat about the

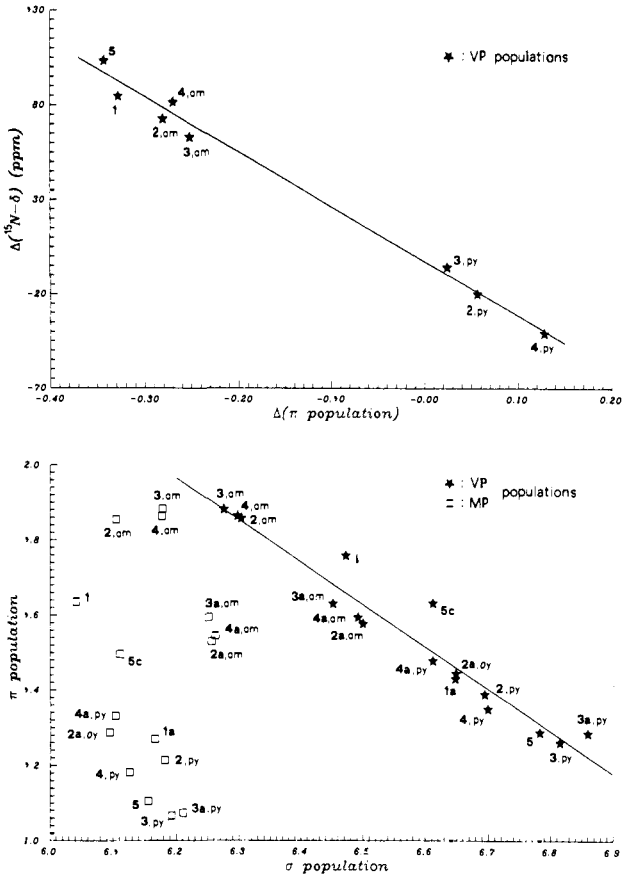

Figure 2. (Top) Correlation between changes in ^{15}N chemical shift [$\Delta(^{15}N-\delta)$] and in virial partitioning (VP) π population [$\Delta(\pi)$] upon deprotonation. (Bottom) Correlation between σ and π electron populations for virial partitioning (VP) and Mulliken partitioning (MP) schemes.

(37) Q is obtained by integration as a nondiagonal 3 × 3 symmetric matrix. Owing to the symmetry of the studied systems, Q matrix factorizes in two blocks of dimension two and one. Thus the unique element associated to the 1 × 1 matrix is automatically a principal component of Q. The average value of the other two diagonal elements equals the average of the other two principal components, since the trace of the matrix is invariant under a similarity transformation.

(38) Press, W. H.; Flammery, B. P.; Teukolsky, S. A.; Vetterling, W. T. *Numerical Recipes. The Art of Scientific Computing*; Cambridge University Press: Cambridge, 1986.

(39) Barzaghi, M.; Simonetta, M. *J. Magn. Reson.* **1983**, *51*, 175.

(40) Hamilton, W. C. *Acta Crystallogr.* **1965**, *18*, 502.

empirical meaning of such correlations is given in the Introduction; the results obtained are detailed here in view of their utility.

Correlations of $(P_\alpha^N)_{VP}$ with Isotropic Shielding $\bar{\sigma}$. As shown in Figure 2, $(P_\sigma^N)_{VP}$ correlates ($r = 0.967$) with $(P_\pi^N)_{VP}$ as do ($r = 0.959$) their changes $(\Delta P_\sigma^N)_{VP}$ and $(\Delta P_\pi^N)_{VP}$ following deprotonation. $(P_\pi^N)_{VP}$ correlates ($r = 0.963$) with ^{15}N experimental chemical shifts δ ($r = 0.963$) and with computed ^{15}N isotropic shieldings $\bar{\sigma}$ ($r = 0.986$); a similar or even better correlation is found for the corresponding differences $(\Delta P_\pi^N)_{VP}$ and $\Delta\delta$ (or $\Delta\bar{\sigma}$) (Figure 2). As $(P_\pi^N)_{VP}$ and $(P_\sigma^N)_{VP}$ correlate with each other, these latter correlate in turn with experimental δ ($r = 0.990$) and computed $\bar{\sigma}$ ($r = 0.984$); namely, upfield (downfield) shifts for increasing P_π^N (P_σ^N) occur. The estimated slopes of $(P_\sigma^N)_{VP}$ versus δ are similar in absolute value, but differ in sign to the ones obtained for $(P_\pi^N)_{VP}$. Hence an increase in total electronic population $(P_T^N)_{VP}$ is generally accompanied by an upfield (downfield) resonance shift when the electronic enrichment results from a gain in P_π^N (P_σ^N), prevailing over the concurrent loss in σ (π) electrons.[41]

Mulliken's populations behave differently as values for $(P_\sigma^N)_{MP}$ do not correlate significantly with $(P_\pi^N)_{MP}$. The nitrogen MP σ populations are, in fact, distributed over a much narrower interval than are the corresponding VP. So while $(P_\pi^N)_{MP}$ correlates with experimental δ and theoretical $\bar{\sigma}$ as do the corresponding changes, no significant correlation is found for $(P_\sigma^N)_{MP}$ and their changes upon deprotonation.

The individual linear correlations of δ (or $\bar{\sigma}$) with P_σ^N and P_π^N do not necessarily imply the existence of a linear correlation between δ (or $\bar{\sigma}$) and the total electron population. In fact, $(P_T^N)_{VP}$ and $(\Delta P_T^N)_{VP}$ are not significantly correlated with δ and $\Delta\delta$, while the corresponding Mulliken populations show an acceptable correlation, despite the lack of a linear correlation between δ and $(P_\sigma^N)_{MP}$. The different behavior is easily explained. In the VP scheme, a linear inverse relationship between P_σ^N and P_π^N with slope close to -1 holds. Conversely, the P_σ^N values are nearly constant in the MP scheme, thus producing a change only in the intercept of the regressed line obtained with the π electron population alone. Comeau et al.,[8] using MP STO-3G ζ scale factor optimized charges and a partial optimization of geometry, found a reasonable correlation between NMR shifts and total charges in substituted pyridines, as well as a linear inverse relationship between P_σ^N and P_π^N. In our study these correlations are not simultaneously met, the VP scheme showing only P_σ^N versus P_π^N linear inverse relationship and the MP scheme conversely displaying total charge versus δ correlation only. Our charges are derived from a diffuse basis set (with the related drawbacks discussed above in the case of MP partitioning scheme), and no Gaussian exponent optimization has been performed, for both VP and MP schemes. Fliszár has pointed out[6,42] that in cases where the variations in charge are small and need to be known with precision (say, e.g., the sp^3 carbons in the alkane series), full optimization of both geometry and scale factors is required. In order to check that VP charges are not as sensitive to ζ scale factor optimization as MP charges, we determined optimum ζ scale factor RHF/STO-3G VP carbon populations for some simple hydrocarbons. The resulting changes in C populations are one or even two orders of magnitude smaller than the corresponding MP changes. For example, in methane, the VP carbon population varies from 5.749 to 5.747 on passing from standard to optimum ζ scale factors while the corresponding MP values are[42,43] 6.263 and 6.049. The negligible sensitivity of VP charges to ζ scale factor optimization,[44] together with their

Table IX. Summary of Linear Correlation Results

electron populations[a]	regressed parameters[b] slope	intercept	goodness of fit measures[c] r	R
	P_σ^N (or ΔP_σ^N) vs P_π^N (or ΔP_π^N)			
VP	-1.12 ± 0.08	9.0 ± 0.5	0.967	0.034
VP(Δ)	-1.5 ± 0.3		0.959	0.212
MP	not significant			
MP(Δ)	not significant			
	P_σ^N (or ΔP_σ^N) vs ^{15}N δ (or ^{15}N $\Delta\delta$) and vs ^{15}N $\bar{\sigma}$ (or ^{15}N $\Delta\bar{\sigma}$)			
exp δ[d]				
VP	$(4.8 \pm 0.2) \times 10^2$	$(-30 \pm 1) \times 10^2$	0.990	0.057
VP(Δ)	$-(4.4 \pm 0.9) \times 10^2$		0.956	0.226
MP	not significant			
MP(Δ)	not significant			
computed $\bar{\sigma}$[e]				
VP	$-(5.3 \pm 0.3) \times 10^2$	$+(35 \pm 2) \times 10^2$	0.984	0.144
VP(Δ)	$-(6.3 \pm 1.5) \times 10^2$		0.941	0.262
MP	not significant			
MP(Δ)	not significant			
	P_π^N (or ΔP_π^N) vs ^{15}N δ (or ^{15}N $\Delta\delta$) and vs ^{15}N $\bar{\sigma}$ (or ^{15}N $\Delta\bar{\sigma}$)			
exp δ[d]				
VP	$-(4.1 \pm 0.3) \times 10^2$	$-(8.2 \pm 0.5) \times 10^2$	0.963	0.108
VP(Δ)	$-(2.8 \pm 0.1) \times 10^2$		0.994	0.081
MP	$-(3.1 \pm 0.1) \times 10^2$	$-(6.5 \pm 0.2) \times 10^2$	0.986	0.064
MP(Δ)	$-(2.4 \pm 0.1) \times 10^2$		0.995	0.075
computed $\bar{\sigma}$[e]				
VP	$(4.5 \pm 0.2) \times 10^2$	$-(6.3 \pm 0.3) \times 10^2$	0.986	0.134
VP(Δ)	$(4.1 \pm 0.3) \times 10^2$		0.986	0.128
MP	$(3.4 \pm 0.1) \times 10^2$	$-(4.3 \pm 0.2) \times 10^2$	0.990	0.114
MP(Δ)	$(3.5 \pm 0.2) \times 10^2$		0.986	0.131
	P_T^N (or ΔP_T^N) vs ^{15}N δ (or ^{15}N $\Delta\delta$) and vs ^{15}N $\bar{\sigma}$ (or ^{15}N $\Delta\bar{\sigma}$)			
exp δ[d]				
VP	not significant			
VP(Δ)	not significant			
MP	$-(3.1 \pm 0.1) \times 10^2$	$(26 \pm 1) \times 10^2$	0.989	0.060
MP(Δ)	$-(3.3 \pm 0.4) \times 10^2$		0.973	0.179
computed $\bar{\sigma}$[e]				
VP	not significant			
VP(Δ)	not significant			
MP	$(3.3 \pm 0.3) \times 10^2$	$-(24 \pm 2) \times 10^2$	0.956	0.241
MP(Δ)	$(4.8 \pm 0.4) \times 10^2$		0.986	0.129
	P_σ^N (or ΔP_σ^N) vs $\bar{\sigma}_{mp}$[f] (or $\Delta\bar{\sigma}_{mp}$)			
VP	$-(9.0 \pm 0.4) \times 10^2$	$(5.9 \pm 0.3) \times 10^3$	0.985	0.167
VP(Δ)	$-(10.0 \pm 0.4) \times 10^2$		0.924	0.302
MP	not significant			
MP(Δ)	not significant			
	P_π^N (or ΔP_π^N) vs $\bar{\sigma}_{mp}$[f] (or $\Delta\bar{\sigma}_{mp}$)			
VP	$(7.7 \pm 0.4) \times 10^2$	$-(12.2 \pm 0.6) \times 10^2$	0.985	0.168
VP(Δ)	$(6.5 \pm 0.5) \times 10^2$		0.982	0.148
MP	$(5.9 \pm 0.2) \times 10^2$	$-(8.7 \pm 0.3) \times 10^2$	0.992	0.123
MP(Δ)	$(5.6 \pm 0.4) \times 10^2$		0.980	0.156
	P_T^N (or ΔP_T^N) vs $\bar{\sigma}_{mp}$[f] (or $\Delta\bar{\sigma}_{mp}$)			
VP	not significant			
VP(Δ)	not significant			
MP	$(5.6 \pm 0.4) \times 10^2$	$-(4.3 \pm 0.3) \times 10^3$	0.965	0.257
MP(Δ)	$(7.7 \pm 0.7) \times 10^2$		0.984	0.140
	P_α^N (or ΔP_α^N) ($\alpha = \sigma, \pi$, or T) vs σ_{op}[g] (or $\Delta\sigma_{op}$)			
	VP, VP(Δ), MP, MP(Δ) all not significant			
	$Q_{op}/\langle r^2\rangle$[h] [or $\Delta(Q_{op}/\langle r^2\rangle)$] vs $(\sigma_{op} - \bar{\sigma})$ [or $\Delta(\sigma_{op} - \bar{\sigma})$]			
VP	$(2.2 \pm 0.1) \times 10^3$	$(5.7 \pm 0.1) \times 10^2$	0.990	0.080
VP(Δ)	$(2.4 \pm 0.2) \times 10^3$		0.960	0.228

[a] VP and MP refer to virial and Mulliken partitioning electron populations, respectively. VP(Δ) and MP(Δ) are the corresponding differences upon deprotonation; P_α^N ($\alpha = \sigma, \pi$, or T for σ, π, and total electron populations) are nitrogen electron populations. [b] Slope in ppm/e and intercept in ppm; "not significant" means that the parameters are not significant on the basis of Student's t-test and of correlation coefficient. [c] r is the correlation coefficient and R is Hamilton's R factor. [d] Linear correlation of P_α^N with the experimental δ values reported in Table VII (δ relative to liquid NH_3). [e] Linear correlation of P_α^N with the computed $\bar{\sigma}$ isotropic shieldings (relative to bare nucleus; see Table VII). [f] Linear correlation between P_α^N and the mean value of shielding in the molecular plane. [g] Linear correlation between P_α^N and the value of shielding perpendicular to the molecular plane. [h] Linear correlation between the component perpendicular (Q_{op}) to the molecular plane of the nitrogen traceless charge density quadrupole moment tensor Q and the deviation of the corresponding component of shielding with respect to $\bar{\sigma}$. Q component is scaled by $1/\langle r_\Omega^2\rangle$ (see text).

(41) Apparently N-py in **3** does not fulfill the above general rule as a downfield shift would be expected on the basis of the corresponding σ population change. However, both P_σ^N and P_π^N rise, in **3**, with σ (0.045 e) prevailing over π (0.022). The observed (−5.3 ppm) or computed (−2.1 ppm) upfield shift is not statistically significant (as it is anticipated by the ΔP_π^N versus $\Delta\delta$ correlation; Figure 2).

(42) Kean, G.; Fliszár, S. *Can. J. Chem.* **1974**, *52*, 2772.

(43) Hehre, W. J.; Stewart, R. F.; Pople, J. A. *J. Chem. Phys.* **1969**, *51*, 2657.

(44) This behavior is but a consequence of a corresponding suitable change in the location of the bcp. A thorough discussion of how bcp moves in dependence on changes in the physical description of a system is given in the paper referred to at the end of footnote 21.

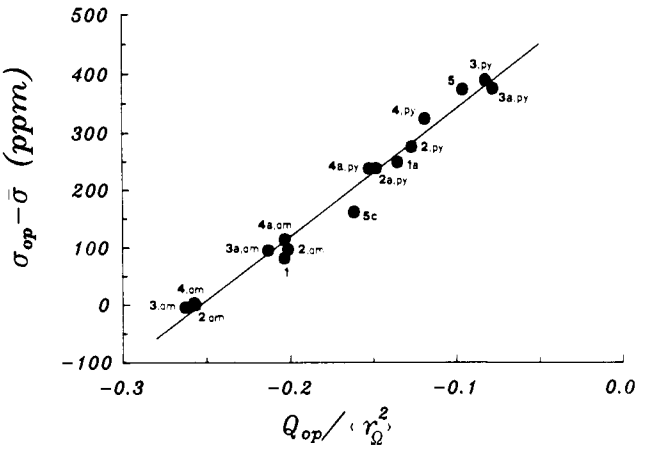

Figure 3. Correlation between the principal component of the nitrogen charge density quadrupole moment tensor perpendicular to the molecular plane (Q_{op}) and the deviation of the corresponding component of shielding with respect to the total ^{15}N isotropic shielding $\bar{\sigma}$. The Q principal component values are scaled by the reciprocal of $\langle r_\Omega^2 \rangle$ (see text).

stability against basis set changes and their ability to describe σ versus π linear inverse relationships, seems to corroborate the existence in these systems of *empirical* linear correlations of δ (or $\bar{\sigma}$) with both σ and π charges, but not with their sum. Escudero et al.[9] used the YSP[45] population analysis scheme in a comprehensive study of the charge distribution of aminopyridines, aminopyrimidines, and some diazine *N*-oxides. They found that total nitrogen charges reflect the corresponding ^{15}N chemical shifts, provided the nitrogen atoms have similar hybridization and substitution patterns. Hence our results suggest that the deprotonated nitrogen, though formally retaining the same hybridization pattern (sp^2) as the protonated one, actually undergoes a significant change in its hybrid orbital compositions. This is also indicated by the aforementioned charge density rearrangements.

Correlations of $(P_\alpha^N)_{YP}$ with the Computed σ Tensor Components. Linear correlations are found for P_α^N with the average value of shielding in the molecular plane. No correlation could be obtained with the out-of-plane component, independently of the partitioning scheme adopted or of the kind ($\alpha = \sigma$, π, or T) of population considered. Correlations with $\bar{\sigma}_{mp}$ show exactly the same pattern recovered above with isotropic $\bar{\sigma}$: in the VP scheme, correlation is found with P_σ^N and P_π^N, while in MP scheme, with P_π^N and P_T^N. The corresponding correlation coefficients are rather good, ranging from 0.924 up to 0.992. The observed parallelism with $\bar{\sigma}$ derives from the near constancy, upon deprotonation, of the σ_{op} component with respect to the significantly greater changes in $\bar{\sigma}_{mp}$. Thus a correlation of P_α^N with $\bar{\sigma}_{mp}$ is not substantially different from a correlation with $\bar{\sigma}$.

Correlations of $(P_\alpha^N)_{YP}$ with the Traceless Charge Density Quadrupole Moment Tensor Components. Q tensor components are available only within the VP scheme. Correlations were obtained with the principal components of the traceless tensor ($\sigma - \bar{\sigma}\mathbf{E}$), where **E** is the 3 × 3 unit matrix. It is to be stressed that if, for example, Q_{op} correlates with ($\sigma_{op} - \bar{\sigma}$), $\bar{Q}_{mp}$ will similarly correlate with ($\bar{\sigma}_{mp} - \bar{\sigma}$), as both **Q** and ($\sigma - \bar{\sigma}\mathbf{E}$) are traceless. The existence of these correlations imply similar correlations between the "mixed" terms also [e.g., Q_{op} versus ($\bar{\sigma}_{mp} - \bar{\sigma}$)]. Therefore, only one relationship is reported in Table IX. The **Q** principal components were scaled by the reciprocal of $\langle r_\Omega^2 \rangle$ in order to eliminate effects due to different total nitrogen electron populations (r_Ω being the atomic electron position vector). Only differences in nitrogen charge density anisotropies are taken into account this way. Rather good correlations were found between both the components of the traceless tensors named above (r = 0.990; see Figure 3) and their changes upon deprotonation (r = 0.960).

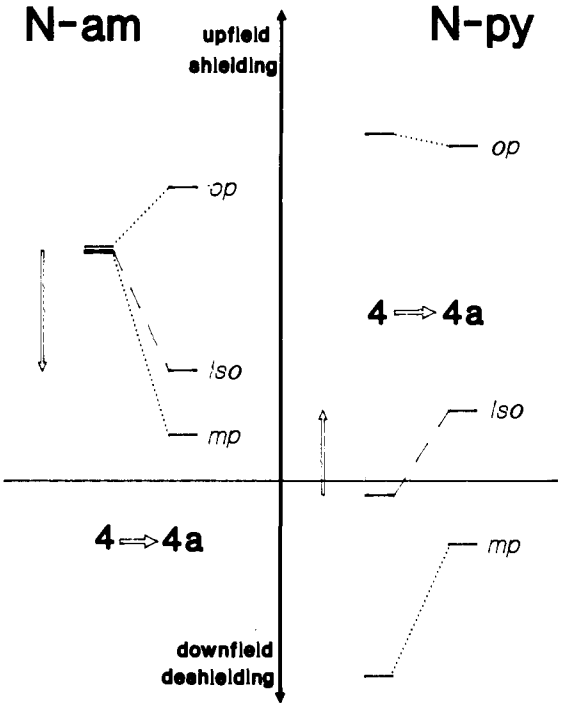

Figure 4. Schematic representation of changes (**4** → **4a**) in isotropic shielding (iso) and in shielding tensor out-of-plane (op) and molecular plane (mp) components.

VI. Conclusions

A coarse-grained analysis shows that the reported[12] dichotomy in the behavior of ^{15}N displacements can be easily rationalized. Indeed, in all the investigated systems, the deprotonated nitrogen undergoes a net electron population decrease (with π loss strongly prevailing over σ increase), whereas the opposite is true in the case of pyridyl nitrogens. According to the linear correlation relating isotropic shifts with electron population values (section V), this charge redistribution induces a downfield ^{15}N NMR resonance shift for the deprotonated nitrogen and an upfield shift for the pyridyl nitrogen.

A deeper physical insight into the problem is obtained when the computed nuclear magnetic shielding anisotropies are inspected (Figure 4). The downfield shift of deprotonated nitrogens results from the dominance of the decrease in shielding in the molecular plane over the concurrent increase [or near constancy (**2a–4a**)] of the out-of-plane shieldings. Conversely, the upfield shift of pyridyl nitrogens is but a consequence of the dominant decrease in deshielding in the molecular plane over the decrease in the out-of-plane shielding. The observed changes in shielding tensor components are mirrored by changes in the Laplacian distribution. This is because the deshielding in the molecular plane is dominated by the magnetic moment generated by the n → π^* excitation, whose importance increases (decreases) as the N lone pair "availability" increases (decreases). A parallel also exists between changes in preferential out-of-plane charge accumulation and shielding tensor anisotropies γ (lower γ values accompanying enhanced out-of-plane charge accumulation for the protonated forms). As an increase in γ is due to a dominant increase in deshielding in the molecular plane, this parallel also implies a correlation between a lowering of the out-of-plane charge accumulation and a concurrent increase in paramagnetic contributions in the molecular plane. Changes in the out-of-plane charge accumulation are then related to changes in π populations, implying a relationship of these latter with the $\bar{\sigma}_{mp}$ changes also. Finally, as $\bar{\sigma}_{mp}$ changes dominate the corresponding out-of-plane changes, isotropic shifts turn out to be related to π populations (or equally

(45) Yánez, M.; Stewart, R. F.; Pople, J. A. *Acta Crystallogr., Sect. A* **1978**, *34*, 641.
(46) Stefaniak, L.; Roberts, J. D.; Witanowski, M.; Webb, G. A. *Org. Magn. Reson.* **1984**, *22*, 201.
(47) Webb, G. A. *Annu. Rep. NMR Spectrosc.* **1986**, *18*, 504.

to P_σ within the VP scheme). The conclusions derived from the empirical analysis reported at the beginning of this section, therefore, have a sounder physical basis.

The changes in VP nitrogen charges following deprotonation agree perfectly with the observed charge redistributions. QTAM allows one to investigate quantitatively these mechanisms, providing also a self-explanatory chemical description of them. Deprotonation of a planar tricoordinated nitrogen increases its σ charge, thereby allowing an efficient release of its π charge to the π-conjugated ring system. So the "increase in σ electron density can be associated with the observed ^{15}N low-field shift"[12] mainly because a greater amount of π charge is pushed away. In fact, the σ electron density made available upon deprotonation at nitrogen is to a great extent transferred to the whole molecular σ framework. Pushing away π charge enables the amino nitrogen to effectively conjugate to the ring π system or, in the case of **1** and **5c** systems, to set up π conjugation throughout all the heterocyclic ring. This is clearly indicated by the differences in the portrait of the Laplacian of the charge density for the protonated and the deprotonated forms.

This study demonstrates that useful and enlightening information is obtained by a combined analysis of changes in nuclear magnetic shielding tensors and charge density rearrangement mechanisms, despite the lack of a firm physical basis relating the two. Moreover, the study shows that apparently intriguing experimental behavior of chemical shift changes upon deprotonation can be rationalized in terms of plain concepts.

Acknowledgment. We thank a referee for his very helpful and stimulating comments. Thanks are also due to Dr. P. J. MacDougall for suggesting that we explore correlations involving the charge density quadrupole moment tensor. The help of Mr. M. Bandera in preparing the drawings is gratefully acknowledged.

Registry No. 1, 109-97-7; **1a**, 23303-09-5; **2**, 504-29-0; **2a**, 41458-22-4; **3**, 462-08-8; **3a**, 80287-52-1; **4**, 504-24-5; **4a**, 37062-09-2; **5**, 110-86-1; **5c**, 16969-45-2.

Substituent Effects. 4. Nature of Substituent Effects at Carbonyl Groups

Kenneth B. Wiberg,*[1a] Christopher M. Hadad,[1a] Paul R. Rablen,[1a] and Jerzy Cioslowski[1b]

Contribution from the Departments of Chemistry, Yale University, New Haven, Connecticut 06511, and Florida State University, Tallahassee, Florida 32306.
Received February 3, 1992

Abstract: The effect of substituents on the properties of acyl derivatives has been examined. Geometry optimizations were carried out at the MP2/6-31G* theoretical level, followed by calculation of energies at the MP3/6-311++G** level. The energies were studied via isodesmic reactions with ethane leading to acetone and a methyl derivative. The calculated energy changes were in good agreement with the available experimental data and showed that groups more electronegative than carbon stabilize a carbonyl group more than methyl, whereas the opposite is true with the more electropositive groups. The reasons for the energy changes were studied by examining bond dissociation energies for the acyl derivatives and for the corresponding methyl derivatives. The changes in electron populations, bond orders, and atom energies that result from changes in substituents were also studied. It is concluded that the stabilization of carbonyl groups by the substituents NH_2, HO, and F results from a combination of two interactions. The first is the interaction of the substituent lone pair with the electron deficient carbonyl carbon, which decreases on going from NH_2 to F. The second is the Coulombic stabilization of dipolar bonds, which increases on going from NH_2 to F. Similar effects are seen with the second-row substituents SH and Cl. The SiH_3 group, along with CN and CF_3, gives a different behavior which results from the positive charge at the substituent atom and the resultant repulsive interaction with the carbonyl carbon. Changes in hybridization also affect the bond dissociation energies, but in a different way than electronegativity.

1. Introduction

The carbonyl group is probably the most important functional group in organic chemistry, and it has received extensive study.[2] Nevertheless, there still remain important questions concerning the nature of the interaction of substituents with this group. One manifestation of this interaction may be seen in the isodesmic reactions in Table I which lists the experimental energies found in replacing a given substituent by a methyl group.[3] Some related reactions have been discussed by George, Bock, and Trachtman.[4] Replacement of a hydrogen by methyl leads to stabilization, whereas the replacement of atoms that are more electronegative than carbon by methyl leads to an endothermic reaction. Another manifestation is found in rotational barriers (Table II) for the bonds joining the carbonyl group to the substituent. Although the barriers are small with methyl groups, they can become quite large with other substituents.

We have carried out an investigation dealing with the ways in which the carbonyl group is affected by the substituents. Here, we have carried out geometry optimizations at the MP2/6-31G* level which is known to give structures close to those determined experimentally.[5] This was followed by MP3/6-311++G** single-point energy calculations. This large basis set is effectively triple-ζ with both diffuse and polarization functions on all atoms, and it includes correction for electron correlation via perturbation theory through the third order. Zero-point energies were estimated via HF/6-31G* frequency calculations. The MP2 wave functions

(1) (a) Yale University. (b) Florida State University.
(2) Cf.: Falbe, J. *Methoden der Organische Chemie (Houben-Weyl)*; Vol. E3, G. Thieme Verlag: Stuttgart, 1983; Vol. E3. Müller, E. *Ibid.* 1973; Vol. 7/7.
(3) The data were taken from: Pedley, J. B.; Naylor, R. D.; Kirby, S. P. *Thermochemical Data of Organic Compounds*; Chapman and Hall: London, 1986.
(4) George, P.; Bock, C. W.; Trachtman, M. *Molecular Structure and Energetics*; VCH Publishers, Florida, 1987; Vol. 4, p 163.
(5) Hehre, W. J.; Radom, L.; Schleyer, P. v. R.; Pople, J. A. *Ab Initio Molecular Orbital Theory*; Wiley: New York, 1986.

0002-7863/92/1514-8644$03.00/0